Environmental Science and Pollution Research (2023) 30:100596–100612
https://doi.org/10.1007/s11356-023-29432-6

RESEARCH ARTICLE

Efficient degradation of the refractory organic pollutant by underwater bubbling pulsed discharge plasma: performance, degradation pathway, and toxicity prediction

Shuai Liu[1] · **Yong Kang**[1] · **Weijie Hua**[1]

Received: 4 July 2023 / Accepted: 17 August 2023 / Published online: 28 August 2023

Abstract

It is essential to develop an efficient technology for the elimination of refractory contaminants due to their high toxicity. In this study, a novel underwater bubbling pulsed discharge plasma (UBPDP) system was proposed for the degradation of Orange II (OII). The degradation performance experiments showed that by enhancing the peak voltage and pulse frequency, the degradation efficiency of OII increased gradually. The removal efficiencies under different air flow rates were close. Reducing OII concentration and solution conductivity could promote the elimination of OII. Compared with neutral and alkaline conditions, acidic condition was more beneficial to OII degradation. The active species including ·OH, $\cdot O_2^-$, $^1O_2$, and hydrated electrons were all involved in OII degradation. The concentrations of O_3 and H_2O_2 in OII solution were lower than those in deionized water. During discharge, the solution pH increased while conductivity decreased. The variation of UV–vis spectra with treatment time indicated the effective decomposition of OII. Possible degradation pathways were speculated based on LC-MS. The toxicity of intermediate products was predicted by the Toxicity Estimation Software Tool. Coexisting constituents including Cl^-, SO_4^{2-}, HCO_3^-, and humic acid had a negative effect on OII removal. Finally, the comparison with other technology depicted the advantage of the UBPDP system.

Keywords Underwater bubbling pulsed discharge plasma · Refractory organic pollutants · Mechanism investigation · Reactive oxygen species · Degradation intermediates · Toxicity prediction

Introduction

With the rapid pace of industrialization of modern society, a great amount of refractory pollutants originated from industrial and agricultural fields are released into the ecosystem (Wang et al. 2022b; Yang et al. 2019), thus posing serious threats for human health and natural environment due to their high toxicity (Zhou et al. 2021a). However, conventional wastewater treatment methods cannot effectively remove the refractory pollutants, which have the properties of strong stability, easy enrichment, and hard biodegradation (Meng et al. 2022; Qiu et al. 2022; Xu et al. 2020; Yang et al. 2019). Thus, it is imperative to develop more promising technologies for the elimination of recalcitrant organics.

Advanced oxidation processes (AOPs) are efficient wastewater technologies for the elimination of refractory pollutants (Chen et al. 2019; Li and Liu 2021; Wu et al. 2012; Yu et al. 2021). AOPs require the incorporation of external input energy and chemical materials to generate various highly reactive substances (Ansari et al. 2021), especially hydroxyl radical (·OH) which is considered as a powerful oxidative species and can non-selectively attack organic pollutant molecules through the abstraction of hydrogen, electron transfer, and electrophilic addition mechanism (Cao et al. 2018; Kumar et al. 2022). AOPs include photocatalysis (Xu et al. 2020), Fenton process (Guo et al. 2021), ozonation (Chen et al. 2021), electrochemical oxidation (Wang et al. 2016b), and sulfate radical–based AOPs (SR-AOPs) (Li et al. 2021a), but several limitations associated with these abovementioned wastewater treatment methods still remain. For example, Fenton oxidation has the disadvantage of narrow pH range,

Responsible Editor: Guilherme Luiz Dotto

✉ Yong Kang
ykang@tju.edu.cn

[1] School of Chemical Engineering and Technology, Tianjin University, Tianjin 300350, China

iron element residual, and the requirement of restoring the wastewater to neutral condition after oxidation (Thomas et al. 2021). For photocatalytic oxidation, most photocatalysts suffer from the defects of poor light utilization, long time treatment, and difficult recovery of catalysts, which restrict their application in the remediation of sewage (Li et al. 2021b; Xiong et al. 2021). Ozonation is regarded as an environment-friendly wastewater purification method, but it has the drawback of limited utilization of O_3 because of the low solubility of ozone in water (Hua et al. 2022; Malik et al. 2020). SR-AOPs would produce a large amount of sulfate ions, which need to be removed, otherwise these sulfate residues would unavoidably threaten the natural environment (Song et al. 2021).

Among all the AOPs, non-thermal plasma technology (NTP) has been identified as a potential method for the degradation of refractory pollutants (Iervolino et al. 2019, Rashid et al. 2020). As one type of NTPs, pulsed discharge plasma (PDP) has attracted extensive attention on the wastewater remediation due to its characteristics of simple operation and high efficiency, as well as it does not require external chemicals for some pollutants which are relatively easily degraded (Guo et al. 2019). When the plasma is triggered, a variety of chemical reactive oxygen species (ROS), such as ·OH, ·H, ·O, HO_2·, H_2O_2, and O_3, accompanied with various physical phenomena including high-energy electrons, ultraviolet light, heat, and shockwave, are generated, which can directly or indirectly act on the molecules of aqueous pollutants (Cao et al. 2018; Hua et al. 2022). Unfortunately, both of the conventional gas-phase and liquid-phase discharge plasma face some obstacles. For instance, the gas-phase discharge plasma suffers from the limited mass transfer rate of gaseous active species through the gas–liquid interface (Zhou et al. 2019), which means the reactive substances cannot effectively diffuse into liquid to oxidize the target pollutant molecules and quickly fade away due to their short half-life (Ma et al. 2021). However, if the plasma is triggered under the water (i.e., liquid-phase discharge plasma) in order to enhance the possibility of collision between active substances and pollutant molecules, the discharge will be affected by the solution conductivity and the electrodes also might be corroded because the electrodes are in contact with the liquid (Hua and Kang 2021).

To address the abovementioned challenges, introducing bubbles into the discharge plasma system is a wise strategy to improve the mass transfer of ROS from gas to the liquid phase (Wright et al. 2019; Zhou et al. 2019), which in turn enhances the concentration of aqueous active species, as well as avoids the contact of electrodes and solution. As illustrated in previous publications, integrating discharge plasma with bubbles can achieve the excellent performance of wastewater treatment and high energy efficiency (Wang et al. 2023a; Zhang et al. 2021; Zhou et al. 2021a; Zhou et al. 2021b). Thus, a novel underwater bubbling pulsed discharge plasma (UBPDP) system whose reactor design is different from conventional gas-phase and liquid-phase discharge plasma is proposed in this study. In the UBPDP system, discharge plasma is ignited in gas phase and produces various ROS, which are injected into liquid phase in the form of bubbles. On one hand, the generated bubbles provide large specific surface area for the gas–liquid interaction, so the active species trapped in bubbles can efficiently permeate into liquid and directly oxidize target pollutant compounds (Zhou et al. 2021a), thus achieving high degradation efficiency. On the other hand, the UBPDP system avoids the drawbacks of electrode corrosion, the effect on discharge by solution conductivity and high energy consumption that exist in liquid-phase discharge. Finally, compared with continuous power supply (AC and DC supply), the nanosecond pulse power supply employed in this work which is characterized by quick rise time and narrow width can provide extremely high instantaneous power density to accelerate electrons and produce strong electric field strength (Shao et al. 2018), thus having higher energy efficiency. However, the academic reports on bubbling plasma driven by pulse power supply for the wastewater remediation are scarce, and little is known about the possible degradation mechanism of refractory pollutants by UBPDP.

Herein, this work aims to investigate the degradation performance and mechanism of refractory contaminations in UBPDP system. Orange II (OII), a typical representative of azo dye (Cai et al. 2016c), was selected as the target refractory pollutant. First, the effects of peak voltage and pulse frequency of pulsed discharge, air flow rate of underwater bubbling, initial OII concentration, initial solution pH, and initial solution conductivity on OII degradation were evaluated. Subsequently, the degradation mechanism of the UBPDP was explored by monitoring the formation of H_2O_2, O_3, and $\cdot O_2^-$ and identifying the role of key ROS via radical trapping experiments. The time evolution of pH and conductivity of the deionized water and OII solution was measured. The degradation process was explored through total organic carbon (TOC) and UV–vis spectra. The degradation pathway of OII in the UBPDP system was proposed based on identified intermediates utilizing liquid chromatography–mass spectrometry (LC-MS). The toxicity of OII and degradation intermediates was also evaluated. The influences of coexistent substances including Cl^-, SO_4^{2-}, HCO_3^-, and humic acid (HA) in the OII solution on the degradation performance of the UBPDP system was examined. Lastly, the UBPDP method was compared with other AOPs for OII degradation.

Experimental

Chemicals

Orange II and indigo were supplied by Maclin. *tert*-Butyl alcohol (TBA) and *p*-benzoquinone (p-BQ) were provided by Aladdin. Potassium titanium oxide oxalate dehydrate and nitroblue tetrazolium (NBT) were purchased from Meryer. Triethylenediamine (TEDA) was supplied by Heowns. Sulfuric acid (H_2SO_4) and sodium chloride (NaCl) were obtained from Rionlon Bohua. and Kermel, respectively. Sodium hydroxide (NaOH) and sodium dihydrogen phosphate (NaH_2PO_4) were purchased from Damao. Anhydrous sodium sulfate (Na_2SO_4) and sodium bicarbonate ($NaHCO_3$) were bought from Jiangtian. All reagents were applied as received without further purification, as well as all experiments associated with water used deionized water.

Experimental setup

Figure 1a depicts the flow chart of the experimental setup, which is composed of pulse power supply, electrical monitoring system, detection/analysis module, and a self-made reactor. The reactor contains a glass sleeve, high-voltage electrodes, a ground electrode, quartz tubes with a hole, and several Plexiglas plates. Five titanium needles (Φ2.0×110.0 mm) serving as high-voltage electrodes were placed in the center of the hollow quartz glass tubes with a length of 80.0 mm and an inner diameter of 3.0 mm, whose bottom one hole with a diameter of 1 mm was located at used for the passage of air to generate underwater bubbles. Air as working gas was injected into the reactor from the top of quartz tubes using an air pump (V-20; Hailea) and flow rate was controlled by a rotameter (LZB-6WB; Shuanghuan). The inner diameter of the glass sleeve was 65 mm, in which OII solution was treated and a circular titanium plate (Φ60.0×2.0 mm) as ground electrode was put. The outer cooling cell of the sleeve with a thickness of 27.5 mm was used to chill down the OII solution to avoid the thermal decomposition of reactive species, and the solution temperature with treatment time showed that the solution temperature enhanced from 21.6 to 33.0 °C when the discharge treatment was completed (Fig. S1 in the Supplementary Information). During each experiment, 100 mL OII solution was discharge treated and Fig. 1b shows the photo of underwater bubbling in the UBPDP system. It can be found that the air went through the holes of quartz tubes to generate bubbles in the solution. When the pulse power was activated, the tiny discharge streamers formed and also passed through the holes and then

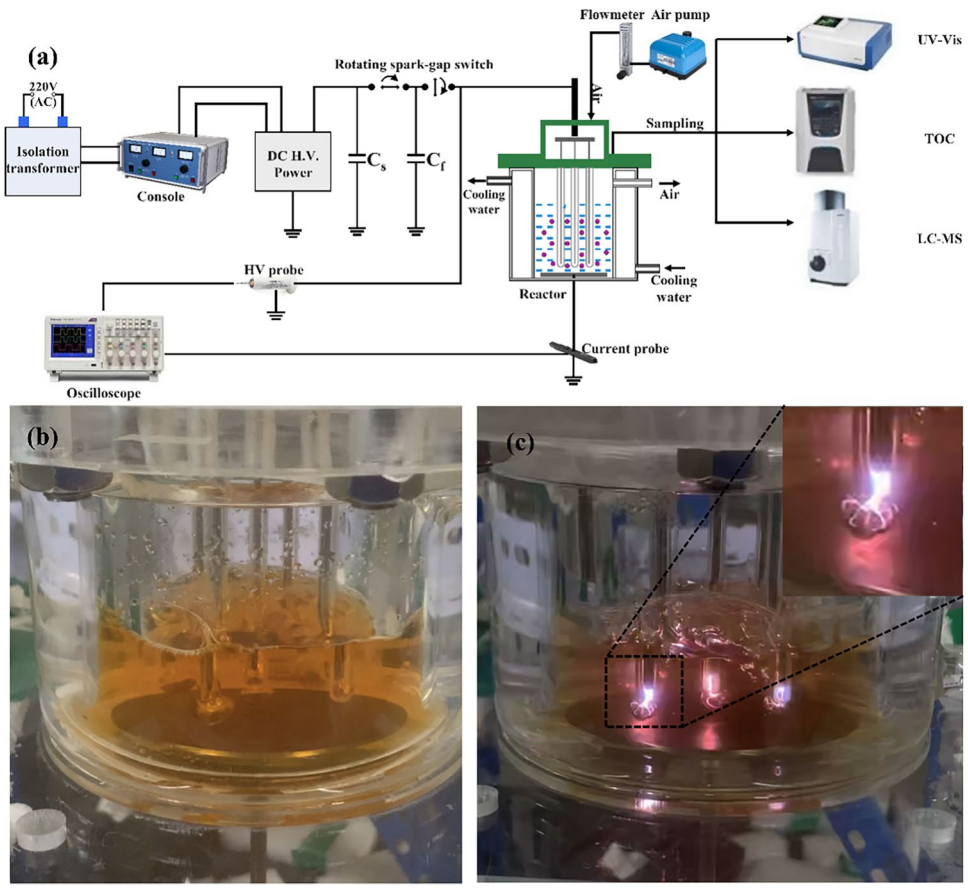

Fig. 1 **a** Schematic diagram of experimental setup; **b** the photo of underwater bubbling in the UBPDP system; **c** the image of underwater bubbling discharge streamer with the power activated

reached the boundary of bubbles, eventually spread in all direction on the bubble surface (Fig. 1c), resulting in the dissociation of water molecules and the formation of ·OH in situ under the strike of high-energy electrons. Figure S2 in the Supplementary Information presents the typical waveforms of pulse voltage and current measured by electrical monitoring system, and the rise time and drop time was about 50 ns and 3 μs, respectively. Other detailed parameters and description of the experimental system are provided in the Supplementary Information.

Analytical method

OII concentration was measured with a UV–vis spectrophotometer (L6S; INESA) at the maximum adsorption peak of 484 nm. The initial pH value was controlled by H_2SO_4 (1.0 mol/L) and NaOH (1.0 mol/L), and the initial conductivity was adjusted by Na_2SO_4. A pH meter (PHS-3C; YOKE) and a conductivity meter (DDSJ-318; INESA) were employed to test the pH and conductivity of solution, respectively. The temperature of treated solution was measured by a digital thermometer (TM902C; SIPEIK). H_2O_2 concentration was determined by the potassium titanium oxalate method through detecting the absorbance at 400 nm (Sellers 1980), and the concentration of aqueous O_3 was measured via the indigo spectrophotometry method (Bader and Hoigné 1981). The concentration of $\cdot O^{2-}$ was determined by the nitroblue tetrazolium transformation method (Goto et al. 2004). The mineralization rate of OII solution was obtained by a total organic carbon (TOC) analyzer (TOC-L; Shimadzu). The intermediate products of OII were determined applying LC-MS (MicrOTOF-Q II; Bruker Daltonics). The toxicity of OII and its degradation intermediates was evaluated by the Toxicity Estimation Software Tool (TEST). The detailed description of indicators of degradation performance, such as degradation efficiency, kinetic constant, and energy efficiency, and the measure conditions of LC-MS are shown in the Supplementary Information.

Results and discussion

Effect of operation parameters on OII degradation

Peak voltage

The pulse peak voltage can determine the energy input and electric field intensity in the reactor, and then affect the formation of active species and intensity of physical effects. Thus, the effect of peak voltage on degradation performance of OII in the UBPDP system was explored and the result is depicted in Fig. 2a. It was shown that a higher peak voltage was conducive to the removal of OII. Under the peak voltage of 17.0, 18.6, 21.0, and 22.8 kV, the degradation efficiency of OII achieved 37.3%, 86.5%, 93.3%, and 95.9% after 30 min of discharge, respectively. The inset of Fig. 2a indicated that OII removal at various peak voltages conformed to the pseudo-first-order kinetic equation. Similarly, a higher kinetic constant was observed under a higher peak voltage. The kinetic constant rose from 0.014 to 0.109 min^{-1} when the peak voltage enhanced from 17.0 to 22.8 kV (Table S1 in the Supplementary Information). Greater peak voltage contributed to the increase of electric field between the high-voltage electrodes and the ground electrode, and then electrons can receive higher energy, which facilitated the formation of active substances including ·OH, $\cdot O^2$, $HO_2\cdot$, H_2O_2, and O_3 (Li et al. 2022; Zhang et al. 2022). In addition, with higher peak voltage, the discharge phenomenon became more obvious and various physical effects such as ultraviolet, shock wave, and heat were more intense, finally promoting the decomposition of OII (Wang et al. 2018).

Energy efficiency is a key indicator, which can reflect energy consumption of the UBPDP system. Higher energy efficiency means that the discharge system is more energy saving. Therefore, the energy efficiencies under different peak voltages were calculated (Fig. S3a in the Supplementary Information). It was worth noting that the energy efficiency rose first and then dropped with the increase of peak voltage. Specifically, under the peak voltage of 17.0, 18.6, 21.0, and 22.8 kV, the energy efficiency reached 181.7, 320.6, 268.2, and 218.1 mg/kW·h after 30 min of treatment, respectively. At the peak voltage of 17.0 kV, the discharge phenomenon was so weak that few active species and physical effects was produced, so the target pollutant was hard to be degraded, resulting in the lowest energy efficiency. However, excessive voltage also led to lower energy efficiency. This is due to the fact that energy efficiency is the ratio of the amount of degraded OII to energy consumption, as shown in Eq. (S3) in the Supplementary Information. When the peak voltage ascended from 18.6 to 22.8 kV, the energy consumption increased significantly, but the amount of OII removal increased relatively slowly. Thus, it is uneconomical to excessively pursue high degradation efficiency by increasing peak voltage. Under the consideration of the balance between degradation efficiency and energy utilization, all subsequent experiments were performed under the peak voltage of 21.0 kV unless otherwise specified.

Pulse frequency

Pulse frequency as a crucial electrical parameter is defined as the number of discharge per second, which is proportional to energy input, thus playing a decisive role on the degradation of OII. Figure 2b displays the influence of pulse frequency on OII elimination. The OII removal efficiency rose with increasing the pulse frequency.

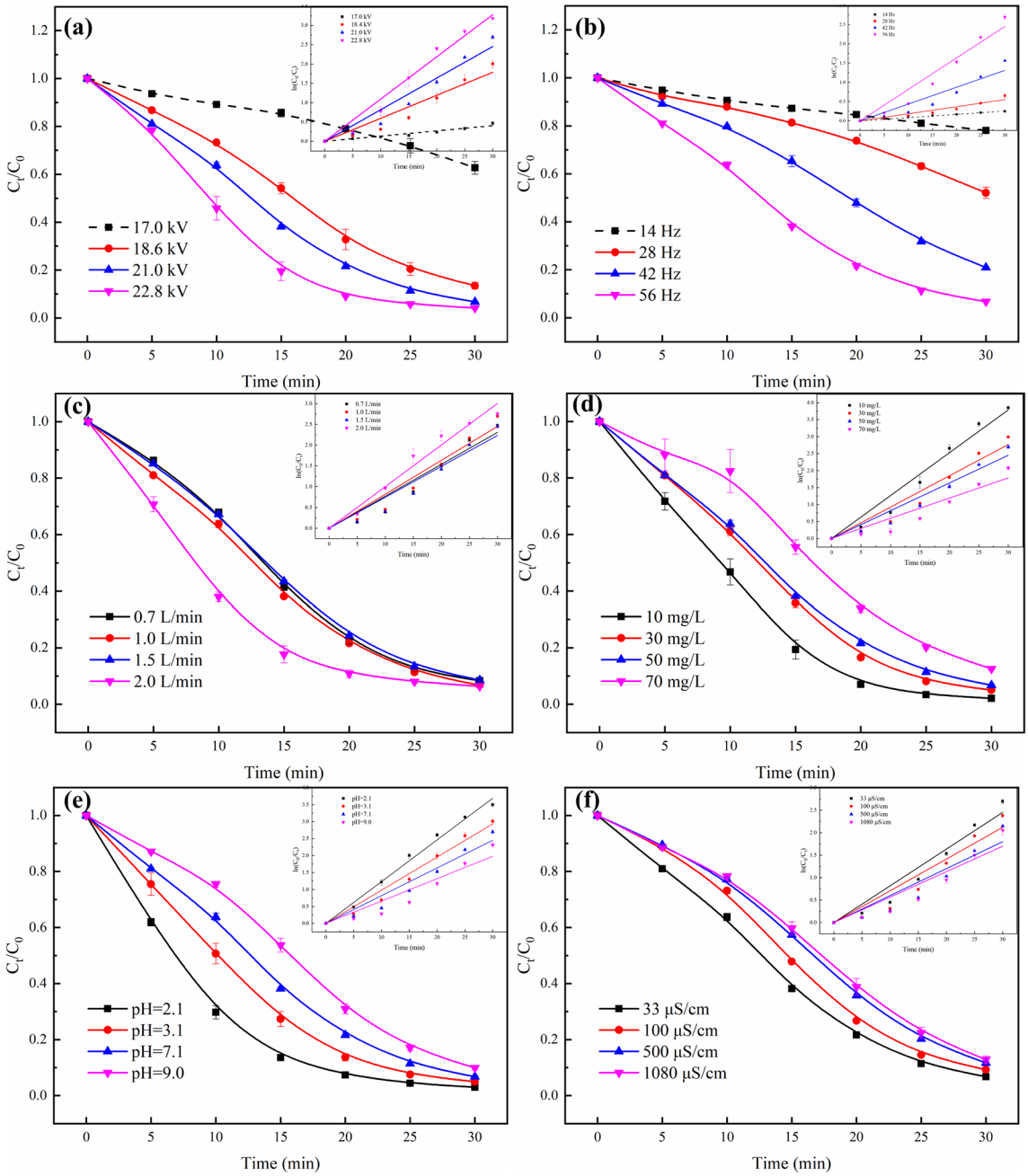

Fig. 2 Effect of operation parameters of the UBPDP system on the OII degradation: **a** peak voltage; **b** pulse frequency; **c** air flow rate; **d** initial OII concentration; **e** initial solution pH; **f** initial solution conductivity

Specifically, 21.9 and 93.3% of OII was removed after 30 min of treatment at a pulse discharge frequency of 14 and 56 Hz, respectively. In addition, the inset of Fig. 2b indicates that the degradation of OII under different pulse frequencies accorded with the pseudo-first-order kinetic equation. As shown in Table S1, the kinetic constant enhanced gradually when increasing the pulse frequency. At the pulse frequency of 56 Hz, the kinetic constant achieved the top value of 0.082 min^{-1}, which was 10.3, 4.6, and 1.9 times as high as those at 14, 28, and 42 Hz, respectively. The reason was that fixed energy was imported into the UBPDP system during one pulse discharge, resulting in fixed amount of physicochemical effects generated, so more active oxidizing substances and physical effects were produced per unit time under a higher pulse frequency, thus enhancing the degradation rate of OII. In addition, the pulse frequency has an effect on the difficulty of ionization of air, and the gas is easier to break

down at a higher frequency, which further facilitates to generate more reactive species (Li et al. 2021b).

The energy efficiency under different pulse frequencies was also inspected (Fig. S3b in the Supplementary Information). The energy efficiency first ascended and then descended as enhancing pulse frequency and the highest energy utilization was obtained at the pulse frequency of 42 Hz. It can be explained by the fact that, at a relatively lower pulse frequency, such as 14, 28, and 42 Hz, boosting pulse frequency can significantly promote the elimination of OII, but the increase of energy consumption was relatively smaller. For instance, when the pulse frequency went up from 14 to 28 Hz, the energy input accordingly doubled; furthermore, the ionization of air was easier to occur with a higher pulse frequency (Li et al. 2021b), causing the amount of generated active species to more than double, which in turn made the quantity of OII degradation increase once above. However, as the pulse frequency increased to 56 Hz, most of the OII was removed when the discharge treatment reached the later stage, so the oxidizing species were more likely to react with the degradation intermediates rather than with the remaining OII. Therefore, at the pulse frequency of 56 Hz, the amount of OII removed per unit input energy declined, resulting in a lower energy efficiency. Although the energy utilization slightly decreased when the pulse frequency enhanced from 42 to 56 Hz, the removal efficiency substantially improved by 14.3%, so the pulse frequency of 56 Hz was selected in the following experiments.

Air flow rate

Air flow rate plays a vital role on the formation of gaseous active species. A low air flow cannot provide sufficient gas molecules especially the oxygen molecules, which are the raw material for producing active substances. An excessive gas velocity would shorten the residence time of oxygen and gaseous active species, leading to the low utilization rate of essential gaseous ROS (Meropoulis et al. 2021). Figure 2c presents the elimination of OII under different air flow rates. It can be seen that there was no distinct difference in removal efficiency because the chosen air flow rates were very close. Notably, the degradation efficiency at the air flow rate of 2.0 L/min was much better than that at other air flow rates in the first 20 min of discharge treatment. Similarly, Table S1 displays that the kinetic constant reaches the highest of 0.100 min^{-1} under the flow rate of 2.0 L/min, indicating that the OII degradation was the fastest at that air flow rate. The reason can be summarized that when the air flow rate was 2.0 L/min, the downward velocity of generated bubbles was fast enough to reach the ground electrode, resulting in the formation of a much brighter and thicker plasma discharge channel between the high-voltage electrodes and ground electrode accompanied by harsh crackling sounds (Fig. S4 in the Supplementary Information). Therefore, more amount of active species and physical effects would be generated from the abovementioned severe discharge phenomenon, which further improved the degradation performance. However, the discharge phenomenon was so intensive that the energy consumption was extremely high and the pulse power supply might be damaged. Thus, 1.0 L/min of air flow rate under which the OII degradation efficiency achieved the highest was adopted in the subsequent experiments.

Initial OII concentration of solution

Initial OII concentration of solution is an important parameter, which can reflect the amount of pollutant in solution. The effect of initial OII concentration on its degradation is demonstrated in Fig. 2d. The OII degradation efficiency and the degradation kinetic constant reduced gradually with raising the initial OII concentration. When the initial OII concentration enhanced from 10 to 70 mg/L, the OII removal efficiency declined from 97.9 to 87.5%, and the degradation kinetic constant declined from 0.126 to 0.059 min^{-1} as shown in Table S1. Whereas a higher initial OII concentration caused more absolute degradation amount. The absolute degradation amount of 6.13 mg was achieved at the initial OII concentration of 70 mg/L after 30 min of discharge, which was about 6.3 times that at 10 mg/L initial OII concentration. Under a fixed peak voltage and pulse frequency, the amount of generated active substances per unit time was generally uniform. When the initial OII concentration of solution increased, the limited amount of active substances was insufficient to completely degrade the higher content of OII, resulting in the reduction of removal efficiency. Nevertheless, with increasing the initial OII concentration, the probability of contact between OII molecules and reactive substances rose, which contributed to a more amount of absolute degradation.

Initial pH of solution

The pH value as a crucial parameter of wastewater treatment can affect the generation and oxidizing ability of active species in the UBPDP system, which in turn has an impact on the elimination of target pollutants. It is therefore significant to investigate the influence of initial solution pH value on OII degradation, and the result is presented in Fig. 2e. The degradation efficiency of OII showed a trend of descending with increasing the initial solution pH, indicating acidic condition was advantageous to the elimination of OII in the UBPDP system, while the degradation of OII was obviously inhibited under alkaline condition. The OII removal efficiency reached the highest of 97.0% at the initial solution pH of 2.1, which was 6.9% higher than that at the pH of 9.0. Similar results were observed in the inset of Fig. 2e and

Table S1. The kinetic constant reduced from 0.123 to 0.066 min^{-1} with the increase of pH from 2.1 to 9.0, which exhibited that OII degradation was faster under acidic condition because of the higher solubility of O_3 under acidic environment, and the direct oxidation of ozone has been regarded as an important mechanism of the degradation of organic pollutants (Magureanu et al. 2018; Sotelo et al. 1989). So, ozone can directly attack OII molecules, resulting in a better degradation performance at a lower pH. Although aqueous ozone molecules can be converted into ·OH under alkaline condition (Eqs. (1) and (2)) (Hua and Kang 2021; Shang et al. 2022), the oxidation capacity of O_3 and ·OH is stronger in acidic solution compared to alkaline condition (Li et al. 2021b). For instance, the redox potential of ·OH changes from 2.70 to 1.90 V when the solution is transformed from acidic condition to alkaline environment, proving that acidic condition is favorable to OII removal (Hua et al. 2022). In addition, OH^- can act as a ·OH scavenger via Eq. (3), inducing a consumption of active species and further adverse to the elimination of OII (Wang et al. 2016a). Thus, the degradation performance of OII was better under the acidic condition and reduced in alkaline solution.

$$OH^- + O_3 \rightarrow \cdot O_2^- + \cdot HO_2 \quad (1)$$

$$O_3 + \cdot HO_2 \rightarrow \cdot OH + 2O_2 \quad (2)$$

$$\cdot OH + OH^- \rightarrow \cdot O^- + H_2O \quad (3)$$

Initial conductivity of solution

The initial conductivity of solution plays an important role on the electric field intensity in the UBPDP reactor and in turn affects the abatement of target pollutants. Thus, it is necessary to find out the effect of initial solution conductivity on OII elimination. As seen in Fig. 2f, the OII degradation efficiency reduced gradually with raising the initial solution conductivity. The OII degradation efficiency reached 93.3% and 87.1% after the discharge treatment of 30 min when the initial solution conductivity was 33 and 1080 μS/cm, respectively. As for the kinetic constant, it decreased from 0.082 to 0.057 min^{-1} when the initial solution conductivity enhanced from 33 to 1080 μS/cm, whose trend was consistent with the degradation efficiency. The phenomenon can be explained by the fact that the higher the solution conductivity, the easier the charge on the high-voltage electrode is drained into the solution, resulting in a smaller potential difference between the electrodes, thus reducing the electric field intensity, which is not conducive to the formation of active substances (Wang et al. 2022a). In conclusion, a higher initial solution conductivity is adverse to OII degradation.

Role of active species

In order to inspect the role of various active species for OII removal, a series of trapping agents were applied in this study. First, TBA was selected to capture hydroxyl radical (·OH) which originated from dissociation, ionization, and excitation of water molecules by high-energy electrons (Eqs. (4)–(8)) (Ansari et al. 2020), and the result is presented in Fig. 3a. It was indicated that the decomposition of OII molecules was significantly suppressed in the presence of TBA, and the inhibitory effect became greater with more TBA added in the solution. To be specific, the removal efficiency of OII declined from 93.3 to 72.5% with the addition of 5 mM. In comparison, when the content of TBA went up to 20 mM TBA, only 53.1% of OII was eliminated after discharge treatment. This was because more ·OH was captured when higher dosage of TBA was added, in turn resulting in a decrease in the oxidative ability of the UBPDP system. Therefore, it can be summarized that ·OH made a decisive contribution for the elimination of OII in UBPDP system.

$$H_2O + e^{-*} \rightarrow \cdot OH + \cdot H + e^- \quad (4)$$

$$H_2O + e^{-*} \rightarrow 2e^- + H_2O^+ \quad (5)$$

$$H_2O + H_2O^+ \rightarrow \cdot OH + H_3O^+ \quad (6)$$

$$H_2O + e^{-*} \rightarrow e^- + H_2O^* \quad (7)$$

$$H_2O + H_2O^* \rightarrow H_2O + \cdot H + \cdot OH \quad (8)$$

Superoxide ion ($\cdot O_2^-$) as one type of important oxidative species can participate in the direct degradation of target pollutant, as well as involve the generation of other active substances (Cabrellon et al. 2020). Previous publications have reported that $\cdot O_2^-$ can be produced in the reaction of O_2 and e^{-*} (Eq. (9)) (Cao et al. 2018).

$$e^{-*} + O_2 + M \rightarrow \cdot O_2^- + M \quad (9)$$

Thus, p-BQ as a typical scavenger of $\cdot O_2^-$ was chosen to evaluate the role of $\cdot O_2^-$ for OII degradation. As seen in Fig. 3b, the addition of p-BQ can obviously inhibit the degradation of OII, and a higher concentration of p-BQ was more restrictive for OII removal. When the concentration of p-BQ enhanced from 0.1 to 1 mM, the reduction of degradation efficiency of OII expanded from 13.2 to 44.9%. This indicated that $\cdot O_2^-$ played a key role for OII abatement.

Singlet oxygen ($^1O_2$) is a type of highly selective oxidant, which can effectively decompose organic pollutants through electrophilic attack and electron extraction (Li et al. 2021b). It is reported that $^1O_2$ can be produced during

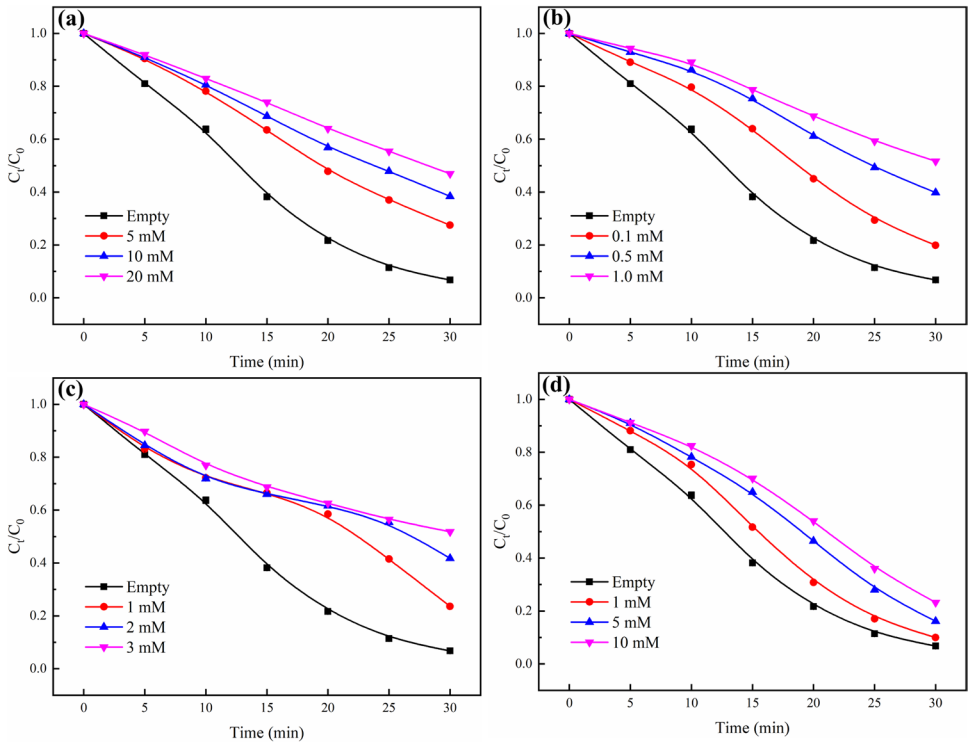

Fig. 3 Effect of the scavengers on OII degradation: **a** TBA; **b** p-BQ; **c** TEDA; **d** NaH_2PO_4

plasma discharge (Wang et al. 2022a). Therefore, in order to study the contribution of $^1O_2$ on OII elimination, TEDA was selected as the trapping agent (Wang et al. 2020). Figure 3c depicts that the OII removal efficiency decreased when the content of TEDA in the solution increased. With the highest concentration of 3 mM TEDA, the OII removal efficiency dropped from 93.3 to 48.2%, illustrating that $^1O_2$ was involved in OII abatement.

During discharge, high-energy electrons can collide with water molecules and form hydrated electrons (e_{aq}) which are directly associated in the degradation of OII or considered as the main medium for the production of active substances (Jiang et al. 2014). Phosphate (NaH_2PO_4) as a common scavenger of e_{aq} was adopted in this study, and the result is shown in Fig. 3d. It can be seen that certain inhibition in OII degradation was detected in the presence of NaH_2PO_4, and the higher the dosage, the more significant was the inhibitory effect on OII removal. With the addition of 10 mM NaH_2PO_4, the OII degradation efficiency reduced from 93.3 to 76.8%. The result suggested that e_{aq} played a certain positive role on OII removal.

Formation of O_3, H_2O_2, and $\cdot O_2^-$

In order to investigate the degradation mechanism of OII in the UBPDP system, the concentration change of aqueous O_3, H_2O_2, and $\cdot O_2^-$ with reaction time was measured. During discharge treatment, high-energy electrons can dissociate O_2 to form ·O, which then react with O_2 to generate O_3 (Eqs. (10) and (11)) (Zhou et al. 2021b). Figure 4a shows the aqueous O_3 concentration in deionized water and OII solution. On one hand, under both reaction conditions,

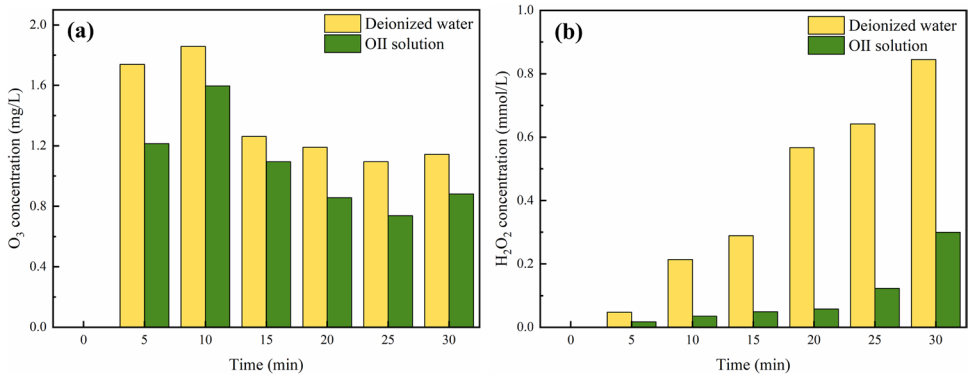

Fig. 4 Variation of **a** O_3 and **b** H_2O_2 concentration in deionized water and OII solution

O_3 concentrations in the late stage of discharge treatment were lower than those in the early stage. O_3 concentration in deionized water were 1.74 and 1.10 mg/L at the discharge time of 5 and 25 min, respectively. This result might be ascribed to increase the solution temperature from 21.6 to 33.0 °C, resulting in a decrease of O_3 solubility. On the other hand, it can be seen that the presence of OII molecules in the solution reduced aqueous O_3 concentration. At the discharge treatment of 30 min, O_3 concentration in deionized water was 1.14 mg/L, and decreased to 0.88 mg/L with the addition of OII, proving that O_3 was consumed by the pollutants. It has been reported that O_3 acts a crucial function on the decomposition of organic contamination through direct and indirect oxidation (Cao et al. 2018; Magureanu et al. 2018). Thus, O_3 as one type of important active species participated in the degradation of OII in UBPDP system.

$$O_2 + e^{-*} \rightarrow 2 \cdot O + e^{-} \tag{10}$$

$$\cdot O + O_2 + M \rightarrow O_3 + M \tag{11}$$

Bombed by high-energy electrons, H_2O is dissociated to generate ·OH, which has an extremely short life span and will quickly combine with each other to form H_2O_2 (Eq. (12)) (Ansari et al. 2020; Hua et al. 2022; Wang et al. 2022a).

$$\cdot OH + \cdot OH \rightarrow H_2O_2 \tag{12}$$

Therefore, the concentration variation of H_2O_2 was investigated, and the result is displayed in Fig. 4b. It was clearly found that the concentration of aqueous H_2O_2 increased with extending discharge treatment time with or without OII molecules, and reached the maximum after 30 min of reaction. In addition, the concentration of H_2O_2 in deionized water was much higher than that in OII solution at the same treatment time. After 30 min of treatment, the concentration of H_2O_2 in deionized water and OII solution reached 0.84 and 0.30 mmol/L, respectively. The result can be explained that ·OH as the precursor of H_2O_2 was substantially consumed to degrade the OII molecules, leading to a decrease of aqueous H_2O_2 concentration in OII solution. Furthermore, H_2O_2 as a common oxidant might be involved in OII removal, which further reduced the concentration of H_2O_2.

As verified in "Role of active species" section, $\cdot O_2^-$ made a marked contribution for the degradation of OII. Thus, the concentration of $\cdot O_2^-$ in deionized water was measured. The concentration of $\cdot O_2^-$ gradually rose as the treatment time increased, and the aqueous $\cdot O_2^-$ concentration reached the maximum of 0.03 mmol/L after 30 min of discharge (Fig. S5 in the Supplementary Information). Nevertheless, the addition of NBT into the OII solution gave rise to the formation of precipitation, indicating that NBT seemed to react with OII molecules, so the concentration of O_2^- in the OII solution was not determined.

Change of pH and conductivity of OII solution

The time evolution of pH and conductivity of deionized water and OII solution with treatment time was explored. No matter if it is deionized water or OII solution, the pH value declined obviously with the discharge treatment going on (Fig. S6 in the Supplementary Information). Especially, the solution pH decreased much faster at the first 10 min of discharge, while it kept relatively stable in the later 20 min. When the air was bubbled into the deionized water and OII solution, N_2 accounted for 78% of air was dissociated by the high-energy electrons and generated nitrogen-related species, which induced the formation of nitrous acid and nitric acid, finally leading to a decrease of pH (Rashid et al. 2020; Topolovec et al. 2022).

Moreover, it was also found that pH in OII solution was lower than that in deionized water. It was indicated that OII molecules could be degraded into small molecular organic acid during discharge treatment, which further decreased the solution pH. As for solution conductivity, it gradually increased as the discharge treatment time prolonged. After 30 min of discharge treatment, the solution conductivity in deionized water and OII solution rose from 2.0 and 33 μS/cm to 652 and 661 μS/cm, respectively. This is due to the fact that the generated NO_2^-, NO_3^-, and hydrate electrons by discharge plasma would enhance the conductivity.

UV–vis spectra and TOC analysis

In order to inspect the degradation process of OII during discharge in the UBPDP system, the UV–vis spectra of the OII solution at different discharge times were measured. The result is presented in Fig. 5a. The UV–vis spectra illustrated that a maximum adsorption peak at 484 nm with a shoulder peak at 430 nm and a main peak at 310 nm existed for the OII solution before discharge treatment. In the visible light range, the typical peak located at 484 nm and the shoulder peak at 430 nm were attributed to the azo linkage in the form of hydrazobenzene structure and azo structure, respectively (Guo et al. 2016). The characteristic peak at 310 nm in ultraviolet light range was related to the naphthalene rings in OII molecules (Wu et al. 2012). As the discharge treatment progressed, all the characteristic adsorption peaks gradually weakened, which indicated that the azo chromophore groups and naphthalene rings were broken down by active species and formed small molecular organic compounds. Whereas the adsorption band between 325 and 375 nm first increased and then decreased with prolonging the treatment time, the adsorption intensity reached the maximum at the treatment time of 20 min. This result proved that some degradation

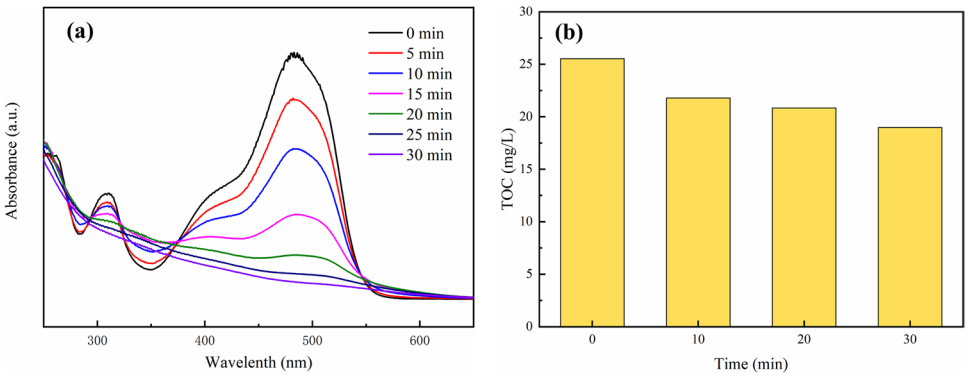

Fig. 5 **a** UV–vis spectra and **b** TOC of the OII solution treated by UBPDP at different discharge times

intermediates were formed and then degraded during discharge. In addition, the decrease of absorbance value in visible region was much more significant than that in ultraviolet range because the azo linkage in the OII molecules was more vulnerable and prone to be attacked by active substances compared to other chemical bonds. After 30 min of treatment, the maximum adsorption peak of the OII solution treated by the UBPDP system in visible light region almost disappeared, implying that OII molecules can be basically removed due to the rupture of azo linkage.

TOC is the carbon content of all organic matter in wastewater. The TOC removal can reflect the mineralization degree of organic compounds. The TOC of the OII solution at different discharge times was examined as depicted in Fig. 5b. Obviously, the TOC of the OII solution decreased gradually with increasing treatment time. The TOC of the initial OII solution was 25.52 mg/L, and at the treatment time of 10, 20, and 30 min, the solution TOC values were 21.79, 20.82, and 18.98 mg/L, with the corresponding TOC removal efficiency of 14.6, 18.4, and 25.6%, respectively. The result indicated that the organic pollutants were oxidized and mineralized into inorganic matter such as H_2O and CO_2. It was also found that TOC removal was substantially lower than the degradation efficiency of OII (93.3% after 30 min of treatment), suggesting that a great amount of degradation intermediates were generated during OII elimination. Considering that the generated intermediate products might have higher toxicities, it is necessary to identify them for OII removal.

Intermediate products and degradation pathways of OII

The intermediate products of OII degradation by the UBPDP system were identified with LC-MS (Fig. S7 and Table S2 in the Supplementary Information). Based on the results and previous publications (Cai et al. 2016a; Cai et al. 2016c; Feng et al. 2020; Guo et al. 2021; Xu et al. 2020), two possible degradation routes were proposed, as displayed in Fig. 6. In the degradation route 1, the degradation process was initiated by the attack of active species on C–N bond of OII due to its weak dissociation energies (Gao et al. 2017), resulting in the production of P1 (m/z = 173) and P2 (m/z = 159). Subsequently, the N=N linkage of P1 was cleaved by the electrophilic addition of ·OH (Cai et al. 2016a), leading to the formation of P3 (m/z = 160). Then, the amino group of P3 was oxidized via electron transfer mechanism and led to the generation of P6 (m/z = 161) (Xu et al. 2020). In the degradation pathway 2, the π bond of N=N in OII molecules was vulnerable and prone to be attacked via electrophilic addition of ·OH, which gave rise to P4 (m/z = 363). Then, the breakage of C–N bond by active species occurred on P4 and caused the production of P2 and P5 (m/z = 207). Similar with P3, the C–N of P5 was disrupted and also brought about the intermediates P6. Not only the hydroxyl groups on P6 could be directly oxidized to ketone group by active substances, but also the naphthalene ring of P6 underwent hydroxylation and resulted in the formation of P8 (m/z = 177), which was further oxidized to generate P9 (m/z = 175). Afterwards, P7 and P9 underwent complicated oxidation and formed two types of five-atom heterocyclic molecules including P10 (m/z = 161) and P11 (m/z = 149), whose five-atom rings were then cut off by the attack of active species and induced the formation of P12 (m/z = 167), P13 (m/z = 195), and P14 (m/z = 181) (Cai et al. 2015). With the rupture of benzene ring, these above-mentioned organic compounds P2, P12, P13, and P14 were oxidized into small molecular carboxylic acid, which were mineralized into H_2O and CO_2 eventually.

Toxicity prediction of OII and its degradation intermediates

Toxicity prediction is of great practical significance for wastewater treatment. The *Daphnia magna* LC_{50} (48 h) and the developmental toxicity of OII and its degradation intermediates were predicted using the TEST (Wang et al. 2023b). The *D. magna* LC_{50} (48 h) refers to 50% lethal concentration after 48 h for *D. magna*. Generally, the higher the *D. magna* LC_{50} (48 h) value, the lower the toxicity of the predicted chemical. As to the developmental toxicity, it refers to the harmful influence of chemicals on the growth

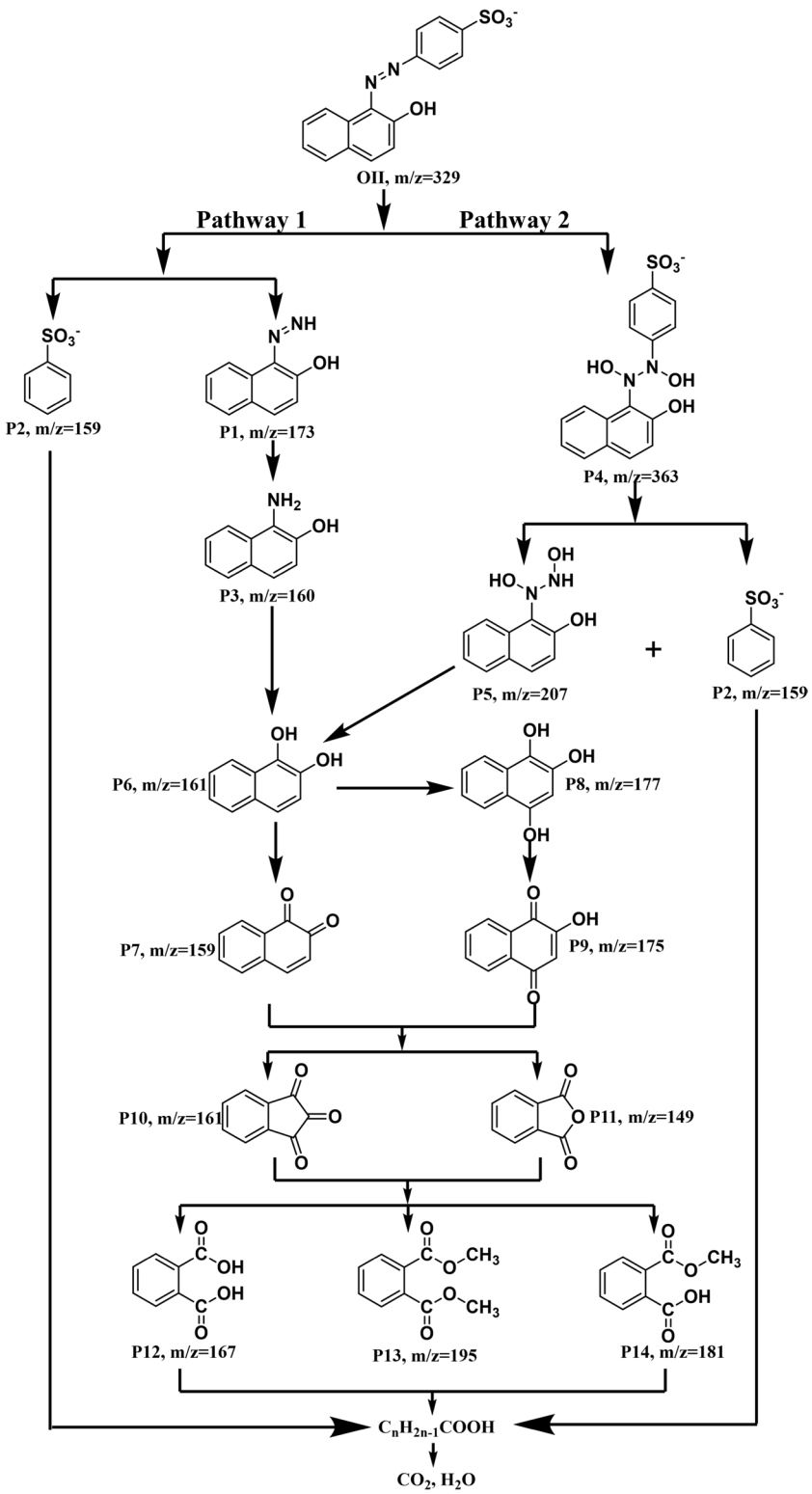

Fig. 6 Degradation pathways of OII in the UBPDP system

and development of immature individuals. As shown in Fig. 7a, all the intermediates had higher *D. magna* LC_{50} (48 h) values compared with OII, indicating that the toxicity of intermediates reduced obviously after discharge treatment. Figure 7b displays that OII had the developmental toxicity of 0.96, meaning that OII was considered as a "developmental toxicant," while nearly all the intermediates except for P4 exhibited a lower developmental toxicity value. Therefore, it can be concluded that the UBPDP treatment method can not only efficiently degrade OII, but also declined its toxicity.

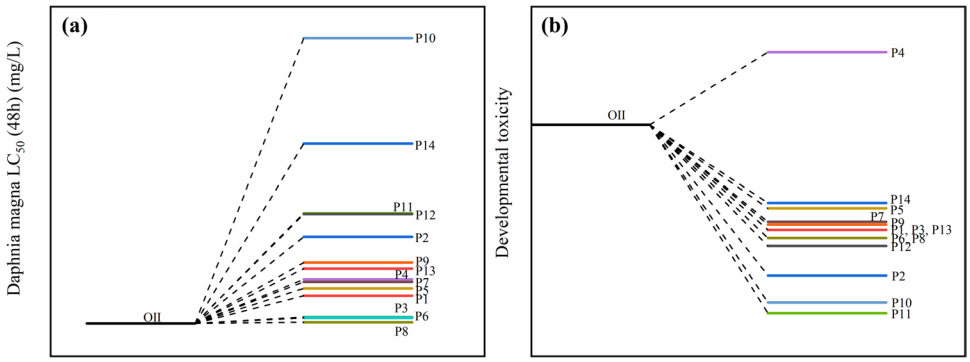

Fig. 7 Toxicity of OII and its degradation intermediates: **a** *Daphnia magna* LC_{50} (48 h); **b** developmental toxicity

Effect of coexisting constituents on OII degradation

In order to assess the degradation performance of UBPDP system in the actual water matrix, some coexisting constituents existing in actual wastewaters including inorganic anions (Cl^-, HCO_3^-, and SO_4^{2-}) and common natural organic compound (humic acid, HA) were chosen to explore their influences on OII degradation. It could be found from Fig. 8a that the presence of Cl^- slightly inhibited the elimination of OII. The removal efficiency of OII reduced from 93.3 to 88.7% when the content of Cl^- went up from 0 to 3 mM. The inhibition effect on OII degradation is due to the fact that Cl^- can quench strongly oxidizing ·OH to produce ·Cl and $\cdot Cl_2$ with lower oxidation abilities (Eqs. (13) and (14)), thus reducing the degradation efficiency of OII (Hua et al. 2022).

$$Cl^- + \cdot OH \rightarrow \cdot Cl + OH^- \tag{13}$$

$$Cl^- + \cdot Cl \rightarrow \cdot Cl_2^- \tag{14}$$

As depicted in Fig. 8b, the addition of HCO_3^- significantly hindered the removal of OII. The degradation efficiency of OII declined by 45.2% with the HCO_3^- concentration of 3 mM. On one hand, HCO_3^- is the common scavenger of ·OH and generates weak reactive substance·CO_3^- (Eq. (15)), resulting in a lower degradation efficiency (Giannakis et al. 2021). On the other hand, the presence of HCO_3^- would alkalize the OII solution, which can be explained by Eq. (16) (Qin et al. 2021). As confirmed in "Initial pH of solution" section, a higher pH value counts against OII degradation, which further reduces the removal efficiency of OII.

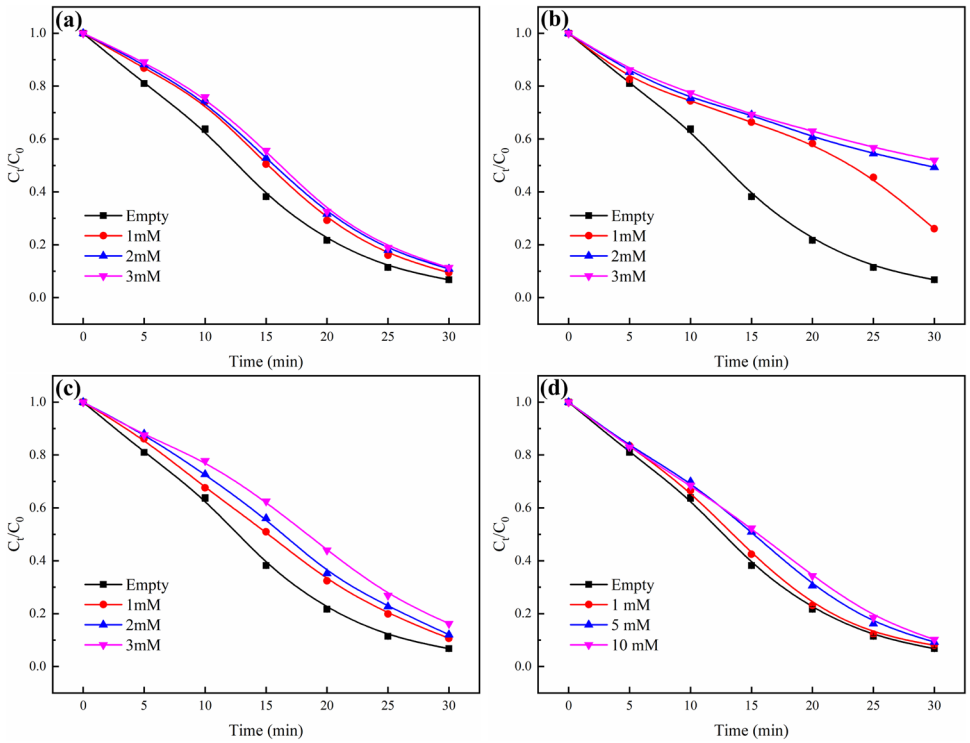

Fig. 8 Effect of coexisting constituents in solution on the degradation of OII: **a** Cl^-; **b** HCO_3^-; **c** SO_4^{2-}; **d** HA

$$HCO_3^- + \cdot OH \rightarrow \cdot CO_3^- + H_2O \quad (15)$$

$$HCO_3^- + H_2O \leftrightarrow H_2CO_3 + OH^- \quad (16)$$

Figure 8c reveals that SO_4^{2-} made a negative contribution on OII degradation. The inhibition effect can be explained by the fact that SO_4^{2-} has the competition with OII molecules (Hu et al. 2021). Figure 8d illustrates that the addition of HA can slightly suppress the abatement of OII. When the concentration of HA rose from 0 to 10 mM, the OII removal efficiency dropped by 3.4%, which was attributed to the competition between HA with target pollutant since HA can consume active species generated from discharge plasma, finally causing a decrease of the OII removal efficiency (Wang et al. 2021). Based on the above results, the conclusions can be drawn that in order to achieve a better performance of OII degradation, inorganic anions and non-target organic matter should be removed before utilizing UBPDP system.

Comparison of UBPDP with other AOPs

In order to explore the characteristics of UBPDP for wastewater treatment, the UBPDP system in this study was compared with other AOPs for OII removal in the literature. As illustrated in Table 1, the removal efficiency of OII by the

Table 1 Comparison of UBPDP with other AOPs for OII degradation

AOPs	OII concentration (mg/L)	Treatment time (min)	Degradation efficiency (%)	Kinetic constant (min^{-1})	Other parameters	Reference
Heterogeneous Fenton	25	120	78	–	[α-FeOOH]: 0.2 g/L; [H_2O_2]: 5 mM; *T*: 30 °C; pH: 3.0	(Tiya-Djowe et al. 2015)
Photo-Fenton	100	60	94.9	0.0468	[$ZnFe_2O_4$]: 0.5 g/L; [H_2O_2]: 5 mM; Xenon lamp power: 150 W; *T*: 20 °C; pH: 6.0	(Cai et al. 2016b)
Ultrasound	50	240	~100	–	Ultrasound frequency: 80 kHz; Electric power: 150 W; *T* = 25 °C	(Velegraki et al. 2006)
Photocatalytic	50	240	98.7	~0.018	[TiO_2]: 0.5 g/L; Mercury lamp power: 125 W; *T*: 22 °C; pH: 6.38	(Kuang et al. 2011)
Catalytic ozonation	50	40	94.1	0.0668	[$MgFe_2O_4$]: 0.1 g/L; Flow rate of ozone: 0.1 L/min; Inlet ozone concentration: 5 mg/L	(Lu et al. 2016)
Electrochemical	100	60	94.96	0.049	[Electrolyte concentration]: 0.1 M; Current density: 40 mA/cm^2; pH: 5	(Xia et al. 2020)
Gliding arc discharge plasma	63	125	99	0.03327	Discharge power: 320 W; Solution flow rate: 20 mL/min; Air flow rate: 800 L/h	(Du et al. 2008)
Dielectric barrier discharge plasma	5	50	35 (DBD) 95 (DBD+PS)	0.0083 (DBD) 0.056 (DBD+PS)	Voltage: 17 kV; frequency: 50 Hz; Discharge power: 2.3–2.5 W	(Shang et al. 2017)
UBPDP	50	30	95.9	0.109	Peak voltage: 22.8 kV; Pulse frequency: 56 Hz; Discharge power: 44 W	This study

heterogeneous Fenton method after 120 min was only 78%, which was lower than that by the UBPDP system. The efficiency of OII degradation by photo-Fenton can reach 94.9%, but the kinetic constant was relatively lower. In addition, AOPs related to Fenton-like methods for the degradation of target pollutant need extrinsic chemical oxidants. Nearly the complete removal of OII was achieved by ultrasound treatment, while it required much longer treatment time (240 min) and relatively higher electric power (150 W). The photocatalytic oxidation of OII exhibited a high degradation efficiency of 98.7%, but it spent a long time (240 min) and the degradation kinetic constant (0.018 min^{-1}) was very small. Another issue of photocatalytic oxidation is that the catalyst powder is of recovery difficulty and may cause secondary pollution (Mozia 2010; Xiong et al. 2021). As for catalytic ozonation, although the removal efficiency and kinetic constant can reach 94.1% and 0.0668 min^{-1}, respectively, which showed outstanding degradation performance, the catalytic ozonation method suffers from the disadvantage of low utilization of O_3 due to the low solubility of ozone in water (Hua et al. 2022; Malik et al. 2020). The electrochemical elimination of OII could achieve a high efficiency of 94.96%, but the drawbacks lie in slow reaction rate (0.049 min^{-1}) and high energy consumption and equipment cost (Feng et al. 2013). Furthermore, UBPDP was compared with other discharge plasma methods. Gliding arc discharge plasma can almost completely eliminate OII, while it required significant energy consumption due to the high discharge power (320 W) and long treatment time (125 min). With regard to dielectric barrier discharge plasma, although its discharge power (2.3–2.5 W) was extremely low compared with gliding arc discharge plasma and UBPDP, the efficiency and kinetic constant of OII removal were only 35% and 0.0083 min^{-1}, respectively, without the addition of persulfate (PS) after 50 min of treatment. In contrast, the discharge power of UBPDP system was relatively lower than other AOPs, and UBPDP could achieve excellent degradation performance without the introduction of external catalysts and oxidants. Specifically, 95.9% of OII was removed by the UBPDP system after 30 min of treatment with only 44 W of discharge power, and the degradation kinetic constant was up to 0.109 min^{-1}, manifesting a good removal performance and low energy consumption.

Conclusion

In this study, a novel method of UBPDP combining bubbles and PDP was developed, which promoted the mass transfer of gaseous ROS into the solution, as well as avoided the shortcoming existing in the liquid-phase discharge plasma, such as electrode corrosion and high energy consumption. The degradation performance of the UBPDP system was assessed by the removal of OII. The effect of operation parameters on OII degradation was investigated. The results showed that boosting peak voltage and pulse frequency was favorable for the elimination of OII. The air flow rate had little influence on degradation performance. The higher removal efficiency was achieved under lower OII concentration, solution pH, and conductivity. It was confirmed that ·OH, $\cdot O_2^-$, $^1O_2$, and e_{aq} were all responsible for the abatement of OII. The concentrations of O_3 and H_2O_2 in the OII solution were all lower than those in the deionized water. The solution pH dropped and conductivity rose when the treatment time was increased. The result of TOC showed a certain mineralization degree of UBPDP system and verified the generation of intermediate products during discharge treatment. The possible degradation pathways were proposed according to the identified intermediates obtained from LC-MS. Then, the toxicity of intermediates was evaluated by TEST. The presence of Cl^-, HCO_3^-, SO_4^{2-}, and HA existing in natural wastewater suppressed the removal of OII in the UBPDP system. Finally, the comparison with other AOPs demonstrates the UBPDP system has the advantages of good degradation performance, and is a potential method for wastewater treatment.

Supplementary Information The online version contains supplementary material available at https://doi.org/10.1007/s11356-023-29432-6.

Author contributions Shuai Liu: conceptualization, methodology, validation, formal analysis, investigation, writing—original draft, writing—review and editing. Yong Kang: resources, supervision, project administration. Weijie Hua: investigation.

Funding No funds, grants, or other support were received.

Data availability The data used or analyzed in this study are available from the corresponding author on reasonable request.

Declarations

Conflict of interest The authors declare no competing interests.

References

Ansari M, Mahvi AH, Salmani MH, Sharifian M, Fallahzadeh H, Ehrampoush MH (2020) Dielectric barrier discharge plasma combined with nano catalyst for aqueous amoxicillin removal: performance modeling, kinetics and optimization study, energy yield, degradation pathway, and toxicity. Sep Purif Technol 251:117270. https://doi.org/10.1016/j.seppur.2020.117270

Ansari M, Sharifian M, Ehrampoush MH, Mahvi AH, Salmani MH, Fallahzadeh H (2021) Dielectric barrier discharge plasma with photocatalysts as a hybrid emerging technology for degradation of synthetic organic compounds in aqueous environments: a critical review. Chemosphere 263:128065. https://doi.org/10.1016/j.chemosphere.2020.128065

Bader H, Hoigné J (1981) Determination of ozone in water by the indigo method. Water Res 15:449–456

Cabrellon G, Tampieri F, Rossa A, Barbon A, Marotta E, Paradisi C (2020) Application of fluorescence-based probes for the determination of superoxide in water treated with air non-thermal plasma. ACS Sens 5:2866–2875. https://doi.org/10.1021/acssensors.0c01042

Cai C, Liu J, Zhang Z, Zheng Y, Zhang H (2016a) Visible light enhanced heterogeneous photo-degradation of Orange II by zinc ferrite ($ZnFe_2O_4$) catalyst with the assistance of persulfate. Sep Purif Technol 165:42–52. https://doi.org/10.1016/j.seppur.2016.03.026

Cai C, Zhang H, Zhong X, Hou L (2015) Ultrasound enhanced heterogeneous activation of peroxymonosulfate by a bimetallic Fe-Co/SBA-15 catalyst for the degradation of Orange II in water. J Hazard Mater 283:70–79. https://doi.org/10.1016/j.jhazmat.2014.08.053

Cai C, Zhang Z, Liu J, Shan N, Zhang H, Dionysiou DD (2016b) Visible light-assisted heterogeneous Fenton with $ZnFe_2O_4$ for the degradation of Orange II in water. Appl Catal B-Environ 182:456–468. https://doi.org/10.1016/j.apcatb.2015.09.056

Cai C, Zhang Z, Zhang H (2016c) Electro-assisted heterogeneous activation of persulfate by Fe/SBA-15 for the degradation of Orange II. J Hazard Mater 313:209–218. https://doi.org/10.1016/j.jhazmat.2016.04.007

Cao Y, Qu G, Li T, Jiang N, Wang T (2018) Review on reactive species in water treatment using electrical discharge plasma: formation, measurement, mechanisms and mass transfer. Plasma Sci Technol 20:103001. https://doi.org/10.1088/2058-6272/aacff4

Chen B, Zhu C, Fei J, Jiang Y, Yin C, Su W, He X, Li Y, Chen Q, Ren Q, Chen Y (2019) Reaction kinetics of phenols and p-nitrophenols in flowing aerated aqueous solutions generated by a discharge plasma jet. J Hazard Mater 363:55–63. https://doi.org/10.1016/j.jhazmat.2018.09.051

Chen H, Zhang ZL, Hu DM, Chen CH, Zhang YX, He SJ, Wang JL (2021) Catalytic ozonation of norfloxacin using Co_3O_4/C composite derived from ZIF-67 as catalyst. Chemosphere 265:129047. https://doi.org/10.1016/j.chemosphere.2020.129047

Du C, Shi T, Sun Y, Zhuang X (2008) Decolorization of Acid Orange 7 solution by gas-liquid gliding arc discharge plasma. J Hazard Mater 154:1192–1197. https://doi.org/10.1016/j.jhazmat.2007.11.032

Feng L, van Hullebusch ED, Rodrigo MA, Esposito G, Oturan MA (2013) Removal of residual anti-inflammatory and analgesic pharmaceuticals from aqueous systems by electrochemical advanced oxidation processes. A review. Chem Eng J 228:944–964. https://doi.org/10.1016/j.cej.2013.05.061

Feng S, Xiao B, Wu M, Wang Y, Chen R, Liu H (2020) Copper phosphide: a dual-catalysis-center catalyst for the efficient activation of peroxydisulfate and degradation of Orange II. Sep Purif Technol 248:117004. https://doi.org/10.1016/j.seppur.2020.117004

Gao B, Chen W, Dong S, Liu J, Liu T, Wang L, Sillanpaa M (2017) Polypyrrole/$ZnIn_2S_4$ composite photocatalyst for enhanced mineralization of chloramphenicol under visible light. J Photoch Photobio A 349:115–123. https://doi.org/10.1016/j.jphotochem.2017.09.018

Giannakis S, Lin K-YA, Ghanbari F (2021) A review of the recent advances on the treatment of industrial wastewaters by sulfate radical-based advanced oxidation processes (SR-AOPs). Chem Eng J 406:127083. https://doi.org/10.1016/j.cej.2020.127083

Goto H, Hanada Y, Ohno T, Matsumura M (2004) Quantitative analysis of superoxide ion and hydrogen peroxide produced from molecular oxygen on photoirradiated TiO_2 particles. J Catal 225:223–229. https://doi.org/10.1016/j.jcat.2004.04.001

Guo H, Jiang N, Wang H, Lu N, Shang K, Li J, Wu Y (2019) Pulsed discharge plasma assisted with graphene-WO_3 nanocomposites for synergistic degradation of antibiotic enrofloxacin in water. Chem Eng J 372:226–240. https://doi.org/10.1016/j.cej.2019.04.119

Guo H, Wang H, Wu Q, Zhou G, Yi C (2016) Kinetic analysis of acid orange 7 degradation by pulsed discharge plasma combined with activated carbon and the synergistic mechanism exploration. Chemosphere 159:221–227. https://doi.org/10.1016/j.chemosphere.2016.05.092

Guo X, Jia J, Xu Y, Meng Q, Zha F, Tang X, Tian H (2021) FeS_2-$Fe_{1-x}S$ heterostructure as a high-efficient Fenton-like catalyst for ultrafast degradation of orange II. Appl Surf Sci 556:149786. https://doi.org/10.1016/j.apsusc.2021.149786

Hu Y, Chen D, Zhang R, Ding Y, Ren Z, Fu M, Cao X, Zeng G (2021) Singlet oxygen-dominated activation of peroxymonosulfate by passion fruit shell derived biochar for catalytic degradation of tetracycline through a non-radical oxidation pathway. J Hazard Mater 419:126495. https://doi.org/10.1016/j.jhazmat.2021.126495

Hua W, Kang Y (2021) Pulsed discharge plasma on water surface coupled with $CaFe_2O_4$/Bi_2O_3 composites for synergistic degradation of aqueous tetracycline hydrochloride. Sep Purif Technol 279:119691. https://doi.org/10.1016/j.seppur.2021.119691

Hua W, Kang Y, Liu S (2022) Synergistic removal of aqueous ciprofloxacin hydrochloride by water surface plasma coupled with peroxymonosulfate activation. Sep Purif Technol 303:122301. https://doi.org/10.1016/j.seppur.2022.122301

Iervolino G, Vaiano V, Palma V (2019) Enhanced removal of water pollutants by dielectric barrier discharge non-thermal plasma reactor. Sep Purif Technol 215:155–162. https://doi.org/10.1016/j.seppur.2019.01.007

Jiang B, Zheng J, Qiu S, Wu M, Zhang Q, Yan Z, Xue Q (2014) Review on electrical discharge plasma technology for wastewater remediation. Chem Eng J 236:348–368. https://doi.org/10.1016/j.cej.2013.09.090

Kuang L, Zhao Y, Liu L (2011) Photodegradation of Orange II by mesoporous TiO_2. J Environ Monit 13:2496–2501. https://doi.org/10.1039/c1em10361j

Kumar A, Skoro N, Gernjak W, Povrenovic D, Puac N (2022) Direct and indirect treatment of organic dye (acid blue 25) solutions by using cold atmospheric plasma jet. Front Phys 10. https://doi.org/10.3389/fphy.2022.835635

Li W, Zhou R, Zhou R, Weerasinghe J, Zhang T, Gissibl A, Cullen PJ, Speight R, Ostrikov K (2022) Insights into amoxicillin degradation in water by non-thermal plasmas. Chemosphere 291:132757. https://doi.org/10.1016/j.chemosphere.2021.132757

Li X, Liu L (2021) Recent advances in nanoscale zero-valent iron/oxidant system as a treatment for contaminated water and soil. J Environ Chem Eng 9:106276. https://doi.org/10.1016/j.jece.2021.106276

Li XD, Shen JL, Sun ZQ, Liu YQ, Zhang WW, Wu B, Ma FJ, Gu QB (2021a) Degradation of 2,4-dinitrotoluene using ferrous activated persulfate: kinetics, mechanisms, and effects of natural water matrices. J Environ Chem Eng 9:106048. https://doi.org/10.1016/j.jece.2021.106048

Li Z, Wang Y, Guo H, Pan S, Puyang C, Su Y, Qiao W, Han J (2021b) Insights into water film DBD plasma driven by pulse power for ibuprofen elimination in water: performance, mechanism and degradation route. Sep Purif Technol 277:119415. https://doi.org/10.1016/j.seppur.2021.119415

Lu J, Wei X, Chang Y, Tian S, Xiong Y (2016) Role of Mg in mesoporous $MgFe_2O_4$ for efficient catalytic ozonation of Acid Orange II. J Chem Technol Biotechnol 91:985–993. https://doi.org/10.1002/jctb.4667

Ma S, Lee S, Kim K, Im J, Jeon H (2021) Purification of organic pollutants in cationic thiazine and azo dye solutions using plasma-based advanced oxidation process via submerged multi-hole dielectric barrier discharge. Sep Purif Technol 255:117715. https://doi.org/10.1016/j.seppur.2020.117715

Magureanu M, Bradu C, Parvulescu VI (2018) Plasma processes for the treatment of water contaminated with harmful organic compounds. J Phys D Appl Phys 51:313002. https://doi.org/10.1088/1361-6463/aacd9c

Malik SN, Ghosh PC, Vaidya AN, Mudliar SN (2020) Hybrid ozonation process for industrial wastewater treatment: principles and applications: a review. J Water Process Eng 35:101193. https://doi.org/10.1016/j.jwpe.2020.101193

Meng FY, Lin CB, Song B, Yu L, Zhao Y, Zhi ZJ, Song M (2022) Synergistic effect of underwater arc discharge plasma and Fe_2O_3-$CoFe_2O_4$ enhanced PMS activation to efficiently degrade refractory organic pollutants. Sep Purif Technol 290:120834. https://doi.org/10.1016/j.seppur.2022.120834

Meropoulis S, Rassias G, Bekiari V, Aggelopoulos CA (2021) Structure-degradation efficiency studies in the remediation of aqueous solutions of dyes using nanosecond-pulsed DBD plasma. Sep Purif Technol 274:119031. https://doi.org/10.1016/j.seppur.2021.119031

Mozia S (2010) Photocatalytic membrane reactors (PMRs) in water and wastewater treatment. A review. Sep Purif Technol 73:71–91. https://doi.org/10.1016/j.seppur.2010.03.021

Qin L, Wang Z, Fu Y, Lai C, Liu X, Li B, Liu S, Yi H, Li L, Zhang M, Li Z, Cao W, Niu Q (2021) Gold nanoparticles-modified $MnFe_2O_4$ with synergistic catalysis for photo-Fenton degradation of tetracycline under neutral pH. J Hazard Mater 414:125448. https://doi.org/10.1016/j.jhazmat.2021.125448

Qiu JL, Li DW, Jing SC, Qiu H, Liu FQ (2022) Advanced technique of catalytic ozonation-enhanced coagulation for the efficient removal of low coagulability refractory organics from secondary effluent. Chemosphere 303:135157. https://doi.org/10.1016/j.chemosphere.2022.135157

Rashid MM, Chowdhury M, Talukder MR (2020) Textile wastewater treatment by underwater parallel-multi-tube air discharge plasma jet. J Environ Chem Eng 8:104504. https://doi.org/10.1016/j.jece.2020.104504

Sellers RM (1980) Spectrophotometric determination of hydrogen peroxide using potassium titanium(IV) oxalate. Analyst 105:950–954

Shang K, Morent R, Wang N, Wang Y, Peng B, Jiang N, Lu N, Li J (2022) Degradation of sulfamethoxazole (SMX) by water falling film DBD plasma/persulfate: reactive species identification and their role in SMX degradation. Chem Eng J 431:133916. https://doi.org/10.1016/j.cej.2021.133916

Shang K, Wang X, Li J, Wang H, Lu N, Jiang N, Wu Y (2017) Synergetic degradation of Acid Orange 7 (AO7) dye by DBD plasma and persulfate. Chem Eng J 311:378–384. https://doi.org/10.1016/j.cej.2016.11.103

Shao T, Wang RX, Zhang C, Yan P (2018) Atmospheric-pressure pulsed discharges and plasmas: mechanism, characteristics and applications. High Volt 3:14–20. https://doi.org/10.1049/hve.2016.0014

Song R, Li H, Kang Z, Zhong R, Wang Y, Zhang Y, Qu G, Wang T (2021) Surface plasma induced elimination of antibiotic-resistant Escherichia coli and resistance genes: antibiotic resistance, horizontal gene transfer, and mechanisms. Sep Purif Technol 275:119185. https://doi.org/10.1016/j.seppur.2021.119185

Sotelo JL, Beltrán FJ, Benitez FJ, Beltrán-Heredia J (1989) Henry's law constant for the ozone-water system. Water Res 23:1239–1246

Thomas N, Dionysiou DD, Pillai SC (2021) Heterogeneous Fenton catalysts: a review of recent advances. J Hazard Mater 404:124082. https://doi.org/10.1016/j.jhazmat.2020.124082

Tiya-Djowe A, Laminsi S, Noupeyi GL, Gaigneaux EM (2015) Non-thermal plasma synthesis of sea-urchin like alpha-FeOOH for the catalytic oxidation of Orange II in aqueous solution. Appl Catal B-Environ 176:99–106. https://doi.org/10.1016/j.apcatb.2015.03.053

Topolovec B, Skoro N, Puac N, Petrovic M (2022) Pathways of organic micropollutants degradation in atmospheric pressure plasma processing - a review. Chemosphere 294:133606. https://doi.org/10.1016/j.chemosphere.2022.133606

Velegraki T, Poulios I, Charalabaki M, Kalogerakis N, Samaras P, Mantzavinos D (2006) Photocatalytic and sonolytic oxidation of acid orange 7 in aqueous solution. Appl Catal B-Environ 62:159–168. https://doi.org/10.1016/j.apcatb.2005.07.007

Wang C, Qu G, Wang T, Deng F, Liang D (2018) Removal of tetracycline antibiotics from wastewater by pulsed corona discharge plasma coupled with natural soil particles. Chem Eng J 346:159–170. https://doi.org/10.1016/j.cej.2018.03.149

Wang H, Mao D, Cao W, Yan X (2020) Analysis of the critical active species for methylene blue decoloration in a dielectric barrier discharge plasma system. Plasma Sci Technol 22:105504. https://doi.org/10.1088/2058-6272/aba345

Wang S, Zhao X, Liu Z, Yang X, Pang B, Gao Y, Zhou R, Xu D, Zhang J, Zhang T, Kong MG (2023a) Violet phosphorus-Fe_3O_4 as a novel photocatalysis-self-Fenton system coupled with underwater bubble plasma to efficiently remove norfloxacin in water. Chem Eng J 452:139481. https://doi.org/10.1016/j.cej.2022.139481

Wang T, Qu G, Ren J, Yan Q, Sun Q, Liang D, Hu S (2016a) Evaluation of the potentials of humic acid removal in water by gas phase surface discharge plasma. Water Res 89:28–38. https://doi.org/10.1016/j.watres.2015.11.039

Wang TY, Zhao C, Meng LH, Li YJ, Chu HY, Wang F, Tao YR, Liu W, Wang CC (2023b) In-situ-construction of BiOI/UiO-66 heterostructure via nanoplate-on-octahedron: a novel p-n heterojunction photocatalyst for efficient sulfadiazine elimination. Chem Eng J 451:138624. https://doi.org/10.1016/j.cej.2022.138624

Wang X, Xu P, Yang C, Shen T, Qu J, Wang P, Zhang G (2021) Enhanced 4-FP removal with $MnFe_2O_4$ catalysts under dielectric barrier discharge plasma: economical synthesis, catalytic performance and degradation mechanism. J Hazard Mater 414:125602. https://doi.org/10.1016/j.jhazmat.2021.125602

Wang Y, Huang J, Guo H, Puyang C, Han J, Li Y, Ruan Y (2022a) Mechanism and process of sulfamethoxazole decomposition with persulfate activated by pulse dielectric barrier discharge plasma. Sep Purif Technol 287:120540. https://doi.org/10.1016/j.seppur.2022.120540

Wang Y, Shen C, Zhang M, Zhang B-T, Yu Y-G (2016b) The electrochemical degradation of ciprofloxacin using a SnO_2-Sb/Ti anode: influencing factors, reaction pathways and energy demand. Chem Eng J 296:79–89. https://doi.org/10.1016/j.cej.2016.03.093

Wang ZM, Xu SH, Cai JZ, Ma JJ, Zhao GH (2022b) Perspective on photoelectrocatalytic removal of refractory organic pollutants in water systems. Acs Es&T Eng 2:1001–1014. https://doi.org/10.1021/acsestengg.1c00443

Wright A, Taglioli M, Montazersadgh F, Shaw A, Iza F, Bandulasena HCH (2019) Microbubble-enhanced DBD plasma reactor: design, characterisation and modelling. Chem Eng Res Des 144:159–173. https://doi.org/10.1016/j.cherd.2019.01.030

Wu J, Zhang H, Qiu J (2012) Degradation of Acid Orange 7 in aqueous solution by a novel electro/Fe^{2+}/peroxydisulfate process. J Hazard Mater 215:138–145. https://doi.org/10.1016/j.jhazmat.2012.02.047

Xia Y, Wang G, Guo L, Dai Q, Ma X (2020) Electrochemical oxidation of Acid Orange 7 azo dye using a PbO_2 electrode: parameter optimization, reaction mechanism and toxicity evaluation. Chemosphere 241:125010. https://doi.org/10.1016/j.chemosphere.2019.125010

Xiong CY, Ren QF, Liu XY, Jin Z, Ding Y, Zhu HT, Li JP, Chen RR (2021) Fenton activity on RhB degradation of magnetic g-C_3N_4/diatomite/Fe_3O_4 composites. Appl Surf Sci 543:148844. https://doi.org/10.1016/j.apsusc.2020.148844

Xu Y, Guo X, Zha F, Tang X, Tian H (2020) Efficient photocatalytic removal of orange II by a Mn_3O_4-FeS_2/Fe_2O_3 heterogeneous catalyst. J Environ Manag 253:109695. https://doi.org/10.1016/j.jenvman.2019.109695

Yang Q, Ma Y, Chen F, Yao F, Sun J, Wang S, Yi K, Hou L, Li X, Wang D (2019) Recent advances in photo-activated sulfate radical-advanced oxidation process (SR-AOP) for refractory organic pollutants removal in water. Chem Eng J 378:122149. https://doi.org/10.1016/j.cej.2019.122149

Yu Y, Wu K, Xu W, Chen D, Fang J, Zhu X, Sun J, Liang Y, Hu X, Li R, Fang Z (2021) Adsorption-photocatalysis synergistic removal of contaminants under antibiotic and Cr(VI) coexistence

environment using non-metal g-C_3N_4 based nanomaterial obtained by supramolecular self-assembly method. J Hazard Mater 404:124171. https://doi.org/10.1016/j.jhazmat.2020.124171

Zhang T, Zhou R, Wang P, Mai-Prochnow A, McConchie R, Li W, Zhou R, Thompson EW, Ostrikov K, Cullen PJ (2021) Degradation of cefixime antibiotic in water by atmospheric plasma bubbles: performance, degradation pathways and toxicity evaluation. Chem Eng J 421:127730. https://doi.org/10.1016/j.cej.2020.127730

Zhang X, Shi P, Zhao W, Lu W, Li F, Min Y, Xu Q (2022) Research on methylene blue degradation based on multineedle-to-plane liquid dielectric barrier discharge mode. Sep Purif Technol 286:120476. https://doi.org/10.1016/j.seppur.2022.120476

Zhou R, Zhang T, Zhou R, Mai-Prochnow A, Ponraj SB, Fang Z, Masood H, Kananagh J, McClure D, Alam D, Ostrikov K, Cullen PJ (2021a) Underwater microplasma bubbles for efficient and simultaneous degradation of mixed dye pollutants. Sci Total Environ 750:142295. https://doi.org/10.1016/j.scitotenv.2020.142295

Zhou R, Zhou R, Alam D, Zhang T, Li W, Xia Y, Mai-Prochnow A, An H, Lovell EC, Masood H, Amal R, Ostrikov KK, Cullen PJ (2021b) Plasmacatalytic bubbles using CeO_2 for organic pollutant degradation. Chem Eng J 403:126413. https://doi.org/10.1016/j.cej.2020.126413

Zhou R, Zhou R, Wang P, Luang B, Zhang X, Fang Z, Xian Y, Lu X, Ostrikov KK, Bazaka K (2019) Microplasma bubbles: reactive vehicles for biofilm dispersal. ACS Appl Mater Interfaces 11:20660–20669. https://doi.org/10.1021/acsami.9b03961